



UNIVERSITY OF LEEDS

This is a repository copy of *A role of enhanced receptor engagement in the evolution of a pandemic acute haemorrhagic conjunctivitis virus*.

White Rose Research Online URL for this paper:  
<http://eprints.whiterose.ac.uk/124791/>

Version: Accepted Version

---

**Article:**

Baggen, J, Hurdiss, DL [orcid.org/0000-0003-3834-5808](https://orcid.org/0000-0003-3834-5808), Zocher, G et al. (17 more authors) (2018) A role of enhanced receptor engagement in the evolution of a pandemic acute haemorrhagic conjunctivitis virus. *Proceedings of the National Academy of Sciences of the United States of America*, 115 (2). pp. 397-402. ISSN 0027-8424

<https://doi.org/10.1073/pnas.1713284115>

---

© 2017, National Academy of Sciences. This is an author produced version of a paper published in *Proceedings of the National Academy of Sciences*. Uploaded in accordance with the publisher's self-archiving policy. In order to comply with the publisher requirements the University does not require the author to sign a nonexclusive licence for this paper.

**Reuse**

Items deposited in White Rose Research Online are protected by copyright, with all rights reserved unless indicated otherwise. They may be downloaded and/or printed for private study, or other acts as permitted by national copyright laws. The publisher or other rights holders may allow further reproduction and re-use of the full text version. This is indicated by the licence information on the White Rose Research Online record for the item.

**Takedown**

If you consider content in White Rose Research Online to be in breach of UK law, please notify us by emailing [eprints@whiterose.ac.uk](mailto:eprints@whiterose.ac.uk) including the URL of the record and the reason for the withdrawal request.



[eprints@whiterose.ac.uk](mailto:eprints@whiterose.ac.uk)  
<https://eprints.whiterose.ac.uk/>

1 **A role of enhanced receptor engagement in the evolution of a pandemic acute haemorrhagic**  
2 **conjunctivitis virus**

3

4 Jim Baggen<sup>a,1</sup>, Daniel L. Hurdiss<sup>b,1</sup>, Georg Zocher<sup>c</sup>, Nitesh Mistry<sup>d</sup>, Richard W. Roberts<sup>a</sup>, Jasper J.  
5 Slager<sup>a</sup>, Hongbo Guo<sup>a</sup>, Arno L. W. van Vliet<sup>a</sup>, Maryam Wahedi<sup>a</sup>, Kimberley Benschop<sup>e</sup>, Erwin Duizer<sup>e</sup>,  
6 Cornelis A.M. de Haan<sup>a</sup>, Erik de Vries<sup>a</sup>, José M. Casasnovas<sup>f</sup>, Raoul J. de Groot<sup>a</sup>, Niklas Arnberg<sup>d</sup>,  
7 Thilo Stehle<sup>c</sup>, Neil A. Ranson<sup>b</sup>, Hendrik Jan Thibaut<sup>a,2</sup>, Frank J. M. van Kuppeveld<sup>a,2,3</sup>

8

9 <sup>a</sup>Virology Division, Department of Infectious Diseases and Immunology, Faculty of Veterinary  
10 Medicine, Utrecht University, 3584CL Utrecht, The Netherlands

11 <sup>b</sup>Astbury Centre for Structural Molecular Biology, Faculty of Biological Sciences, University of Leeds,  
12 Leeds LS2 9JT, UK

13 <sup>c</sup>Interfaculty Institute of Biochemistry, University Tübingen, 72076 Tübingen, Germany

14 <sup>d</sup>Division of Virology, Department of Clinical Microbiology, Umeå University, 90187 Umeå, Sweden

15 <sup>e</sup>Centre for Infectious Disease Control, National Institute for Public Health and the Environment,  
16 3720BA Bilthoven, The Netherlands

17 <sup>f</sup>Centro Nacional de Biotecnología (CNB-CSIC), Darwin 3, Campus Universidad Autónoma de  
18 Madrid, 28049 Madrid, Spain.

19

20 <sup>1</sup>J.B. and D.L.H. contributed equally to this work

21 <sup>2</sup>H.J.T. and F.J.M.v.K. contributed equally to this work

22 <sup>3</sup>To whom correspondence may be addressed. E-mail: f.j.m.vankuppeveld@uu.nl.

23

24 Keywords: conjunctivitis, coxsackievirus A24v, receptor, ICAM-1, sialic acid

25

26 **Author contributions.** Conceptualization, J.B., H.J.T. and F.J.M.v.K.; Infectivity/binding assays, J.B.,  
27 N.M., R.W.R., J.J.S., M.W., and H.J.T.; cryo-EM, D.L.H., G.Z., and N.M.; Mutant virus production,  
28 A.L.W.v.V. and M.W. Phylogenetic analysis, J.B. Bio-layer interferometry, H.G.; Virus isolation and  
29 sequencing, K.B. and E.D.; Resources, C.A.M.d.H., and J.M.C.; Writing – Original Draft, J.B, D.L.H.,  
30 H.J.T. and F.J.M.v.K.; Writing – Review & Editing, G.Z., N.M., E.d.V., J.M.C., R.J.d.G., N.A., T.S.,  
31 and N.A.R.; Supervision, E.d.V., R.J.d.G., N.A., T.S., N.A.R., H.J.T., and F.J.M.v.K; Funding  
32 Acquisition, D.L.H., G.Z., N.A., T.S., N.A.R., and F.J.M.v.K.

33

34 Acute haemorrhagic conjunctivitis (AHC) is a painful, contagious eye disease, with millions of cases in  
35 the last decades. Coxsackievirus A24 (CV-A24) was not originally associated with human disease, but  
36 in 1970 a pathogenic “variant” (CV-A24v) emerged, which is now the main cause of AHC. Initially,  
37 this “variant” circulated only in Southeast Asia, but it later spread worldwide, accounting for numerous  
38 AHC outbreaks and two pandemics. While both CV-A24 “variant” and “non-variant” strains still  
39 circulate in humans, only “variant” strains cause AHC for reasons that are yet unknown. Since  
40 receptors are important determinants of viral tropism, we set out to map the CV-A24 receptor repertoire  
41 and establish whether changes in receptor preference have led to the increased pathogenicity and rapid  
42 spread of CV-A24v. Here, we identify ICAM-1 as an essential receptor for both AHC-causing and non-  
43 AHC strains. We provide the first high-resolution cryo-EM structure of a virus-ICAM-1 complex,  
44 which revealed critical ICAM-1-binding residues. These data could help identify a possible conserved  
45 mode of receptor engagement among ICAM-1-binding enteroviruses and rhinoviruses. Moreover, we  
46 identify a single capsid substitution that has been adopted by all pandemic CV-A24v strains and we  
47 reveal that this adaptation enhances the capacity of CV-A24v to bind sialic acid. Our data elucidate the  
48 CV-A24v receptor repertoire and point to a role of enhanced receptor engagement in the adaptation to  
49 the eye, possibly enabling pandemic spread.

50

#### 51 **Significance statement**

52 Acute haemorrhagic conjunctivitis (AHC) is a painful and highly contagious infection of the eye, with  
53 reported incidence rates of up to 48%. No drugs or vaccines are available for treatment or prevention of  
54 AHC. Coxsackievirus A24 variant (CV-A24v) is the main etiological agent of AHC, being responsible  
55 for >10 million AHC cases worldwide during the last decades. We have identified the CV-A24v  
56 protein receptor and determined the high-resolution structure of the virus-receptor complex.  
57 Furthermore, we found that an adaptation which enhances binding to the receptor sialic acid may have  
58 contributed to the pathogenicity and pandemic nature of CV-A24v. These findings highlight the  
59 importance of sialic acid for viruses with ocular tropism, such as influenza A virus and several  
60 adenoviruses.

61 \body

## 62 **Introduction**

63 Acute haemorrhagic conjunctivitis (AHC) is characterized by a sudden onset of ocular pain, swelling,  
64 watering and extensive subconjunctival haemorrhaging. Since AHC is highly contagious, it spreads  
65 rapidly and can affect up to 48% of a population in a single outbreak (1, 2). Coxsackievirus A24 variant  
66 (CV-A24v), belonging to the genus Enterovirus within the family Picornaviridae, is the main  
67 etiological agent of AHC, being responsible for >10 million AHC cases worldwide during the last  
68 decades (2, 3). Coxsackievirus A24 (CV-A24) was first isolated in South Africa in 1951 (4), but was  
69 not associated with disease in humans. However, in 1970, a pathogenic variant of CV-A24 (CV-A24v)  
70 emerged that was responsible for a large AHC outbreak in Singapore (5, 6). Initially, this AHC-causing  
71 variant circulated only in Southeast Asia, but later spread worldwide, suddenly causing numerous  
72 explosive AHC outbreaks and two pandemics, which started in 1985 and 2002 (7–9). Although both  
73 the CV-A24 variant and non-variant strains are being detected in clinical samples worldwide, only  
74 strains belonging to the “variant” clade are associated with AHC. As yet, the molecular mechanism  
75 underlying this difference in pathogenicity is unknown. Also, it remains unclear what has led to the  
76 sudden onset of CV-A24v pandemics.

77

78 Receptor choice or the interplay between different receptors can be important determinants of viral  
79 tropism and pathogenicity. Most enteroviruses rely on an uncoating receptor that triggers destabilizing  
80 rearrangements of the capsid proteins, resulting in the formation of a capsid-mediated pore in the  
81 endosomal membrane through which the viral genome is delivered into the cytoplasm (10). In addition  
82 to uncoating receptors, many enteroviruses employ one or more attachment receptors that do not  
83 participate in uncoating but facilitate cell binding. Previous reports have shown that sialic acid (Sia)  
84 plays a role in infection of CV-A24v (11). Despite these findings, it remains unclear whether CV-A24v  
85 requires additional cell surface receptors and whether differences in receptor preference exist between  
86 AHC- and non-AHC-causing CV-A24 strains.

87

88 In this study, we set out to identify a potential protein receptor and to investigate if possible changes in  
89 receptor requirements can explain the pathogenic and pandemic nature of AHC-causing CV-A24v  
90 strains. We identify ICAM-1 as an essential receptor for both AHC- and non-AHC-causing CV-A24  
91 strains and provide the first high-resolution cryo-EM structure of a virus in complex with ICAM-1,  
92 revealing in detail the interactions between CV-A24v and its receptor. Moreover, by combining  
93 structural data, phylogenetic analysis and reverse genetics, we identify a single amino acid substitution  
94 in the viral capsid that provides an improved Sia binding capacity and has been adopted exclusively by  
95 pandemic CV-A24 “variant” strains. These findings point towards a role of enhanced Sia binding in the  
96 adaptation of CV-A24v to the eye, which may have been a prerequisite for its pandemic potential.

97

98 **Results**

99

100 **ICAM-1 is an essential CV-A24v receptor**

101 CV-A24v can bind Sia, but Sia was not found to initiate uncoating (12), suggesting that CV-A24v  
102 employs an additional, yet unknown, receptor. In order to identify this receptor, we performed  
103 neutralization assays with a CV-A24v clinical isolate in Sia-deficient HAP1 CMAS<sup>KO</sup> cells (13), using  
104 soluble receptor domains (VLDL-R) or antibodies targeting various known enterovirus receptors  
105 (ICAM-1, DAF, integrin  $\alpha$ 2, PVR, CAR, integrin  $\alpha$ v $\beta$ 3, and PSGL-1) (**Fig. 1A**). The ability of these  
106 ligands to suppress receptor binding was confirmed using positive control viruses (**Fig. S1A**). Only the  
107 antibody against ICAM-1, a cell adhesion molecule consisting of five Ig-like domains (14) (**Fig. 1B**),  
108 blocked CV-A24v infection (**Fig. 1A**). To determine whether ICAM-1 is essential for CV-A24v, we  
109 knocked out ICAM-1 in various cell types by CRISPR/Cas9 genome editing (**Fig. 1B**). The ICAM-1  
110 knockout (ICAM-1<sup>KO</sup>) genotype was verified by sequence analysis (**Fig. S1B**) and by assessing the  
111 susceptibility of ICAM-1<sup>KO</sup> cells to infection with ICAM-1-dependent coxsackievirus A21 (CV-A21)  
112 (15) and rhinovirus B14 (RV-B14) (16), and CAR-dependent coxsackievirus B3 (CV-B3) (17) (**Fig. 1**  
113 **F and G and S1 C-E**). CV-A24v infection was reduced by ICAM-1 knockout in HAP1 CMAS<sup>KO</sup> cells  
114 (**Fig. S1C**), wt HAP1 cells (**Fig. S1D**), as well as HeLa cells (**Fig. 1C**), and was rescued by transfecting  
115 ICAM1 cDNA (**Fig. 1C**). Bio-layer interferometry (**Fig. 1D**) and CV-A24v neutralization with soluble  
116 ICAM-1 ectodomain in primary conjunctival cells (**Fig. 1E**) pointed to a direct interaction between  
117 CV-A24v and ICAM-1. Analysis of virus production in HeLa cells (**Fig. 1F**) and analysis of cytopathic  
118 effect induction in HeLa (**Fig. 1G**) or human corneal epithelial (HCE) cells (**Fig. S1E**) showed that  
119 several CV-A24v clinical isolates, the non-variant prototype strain Joseph, and a non-variant clinical  
120 isolate all require ICAM-1 for infection. Sialylation of ICAM-1 was not found to be essential for  
121 interaction with CV-A24v and CV-A24 Joseph, as shown by bio-layer interferometry (**Fig. S1F**).  
122 Taken together, these data indicate that ICAM-1 functions as an essential receptor for AHC-causing  
123 variant strains as well as non-variant strains.

124

125 **The structure of CV-A24v in complex with ICAM-1**

126 To elucidate the molecular interaction of CV-A24v with ICAM-1, we determined the structure of a  
127 complex between purified virions and a recombinant D1-D2 fragment of ICAM-1 (**Fig. 2 A and B and**  
128 **Table S1**). CV-A24v virions were immobilized on a lacey carbon support after which D1-D2 was  
129 added 30 seconds at 8 °C prior to blotting and plunge freezing. This rapid on-grid binding approach  
130 allowed us to capture the cryo-EM structure of CV-A24v with bound D1-D2, whereas longer  
131 incubation resulted in loss of particle integrity, probably due to receptor-mediated destabilization of the  
132 particle. The global resolution of the EM density is 3.9 Å (**Fig. S2 A-D**), the resolution of the viral  
133 capsid proteins ~3.6-3.8 Å and that of the capsid-interfacing region of ICAM-1 D1 ~3.7 Å (**Fig. S2 E-**  
134 **H**), sufficient to resolve bulky side chains in the electron density map (**Fig. 2C**). The surface of an  
135 enterovirus particle is comprised of 60 copies of the structural proteins VP1, VP2, and VP3 (**Fig. 2A**).  
136 A depression encircling each five-fold axis of symmetry forms the so-called ‘canyon’, which is the  
137 binding site for all uncoating receptors identified to date. The structure shows that the D1 domain binds  
138 in the canyon at the quasi-threefold axis of the capsid (**Fig. 2B**). In contrast to earlier studies, the

139 interface between the capsid and ICAM-1 D1 is well defined in the final EM density map, enabling us  
140 to resolve secondary structure and the majority of side chains in this portion of the structure. This, in  
141 turn, allowed us to calculate an accurate footprint of the D1 component of the receptor on the virus  
142 surface, shown as a 'roadmap' projection (**Fig. 2D**). The specificity in the interaction between ICAM-1  
143 and CV-A24v is largely driven by electrostatic complementarity (**Fig. 2E and S2I**). Specifically, Lys<sup>29</sup>  
144 (FG loop) of ICAM-1 interacts with VP3 Asp<sup>181</sup> and VP1 Asp<sup>238</sup> (**Fig. 2F and S2J**). In addition, Asp<sup>71</sup>  
145 on the tip of the FG loop of ICAM-1 forms a salt bridge with VP1 Arg<sup>168</sup>. Finally, Lys<sup>50</sup> (strand C) and  
146 Lys<sup>39</sup> (strand D) of ICAM-1 form salt bridges with VP1 Asp<sup>228</sup> and Asp<sup>225</sup> (GH loop). Additional  
147 interactions include a hydrogen bonding network that tethers the DE loop of ICAM-1 D1 (Arg<sup>49</sup>, Asn<sup>47</sup>  
148 and Pro<sup>45</sup>) to VP1 (Tyr<sup>230</sup>) and VP2 (Ala<sup>138</sup>, Lys<sup>139</sup> and Thr<sup>140</sup>) (**Fig. S2K**). Many of these residues are  
149 conserved among other ICAM-1-binding viruses belonging to the enterovirus C species, suggesting a  
150 conserved mode of interaction with ICAM-1 (18). On the contrary, only VP1 Asp<sup>238</sup> and VP3 Asp<sup>181</sup>  
151 are present in ICAM-1-binding rhinoviruses.

152

### 153 **Sia is an attachment receptor supporting ICAM-1-mediated CV-A24v infection**

154 In addition to their uncoating receptor, several enteroviruses exploit additional receptors to enhance cell  
155 attachment. Since previous studies identified a role of Sia for CV-A24v (11, 12), we set out to  
156 investigate how Sia and ICAM-1 cooperate during CV-A24v infection. Removal of cell-surface Sia by  
157 CMAS knockout or NA treatment revealed that Sia supports CV-A24v infection (**Fig. 3A and S3A**).  
158 The role of Sia was more prominent when infection was performed on ice, compared to infection at  
159 37°C (**Fig. 3A**). This may be due to stabilization of the interaction at low temperature, as was  
160 previously described for several other Sia-binding viruses (19, 20). NA treatment of several cell types  
161 revealed that Sia supports CV-A24v infection of HCE and HAP1 cells, but not of HeLa cells (**Fig. 3B**).  
162 This difference might result from variability in the expression levels of ICAM-1/Sia or in the types of  
163 Sia expressed on cells. Sia removal from HCE cells (**Fig. 3C and 3D and S3B**) or HAP1 cells (**Fig.**  
164 **S3C**) incompletely inhibited CV-A24v infection, whereas knockout of ICAM-1 completely blocked  
165 CV-A24v infection (**Fig. 3D**). Analysis of virus binding to HCE cells (**Fig. 3E**) and primary  
166 conjunctival cells (**Fig. 3F**) showed that Sia plays a role in cell attachment of CV-A24v. Together,  
167 these results show that, while ICAM-1 is the main CV-A24v receptor, Sia functions as an auxiliary  
168 attachment receptor.

169

### 170 **Differential Sia dependency between AHC-causing strains and non-AHC strains**

171 Next, we tested whether AHC strains and non-AHC strains differ in their dependency on cell surface  
172 Sia, either by treating HCE cells with NA to remove Sia (**Fig. 4A and S4A**) or with NaIO<sub>3</sub> to oxidize  
173 carbohydrates (**Fig. S4B**). The AHC strains were more reliant on Sia than a non-AHC clinical isolate  
174 and the non-AHC prototype strain Joseph. Comparison of VP1 residues that constitute the Sia-binding  
175 site (12) showed that only one residue present in all AHC strains (VP1 Tyr<sup>250</sup>) was absent in the non-  
176 AHC strains (VP1 Phe<sup>250</sup>) (**Fig. 4B**). Although a Sia-binding site lacking this residue might be  
177 functional, the presence of Tyr<sup>250</sup> could increase the affinity by hydrogen bonding with the 5-N-acyl

178 carbonyl group in Sia (**Fig. 4C**). A similar mode of Sia stabilization is seen in other viral lectins, such  
179 as coronavirus hemagglutinin-esterases (20) and influenza neuraminidases (19) (**Fig. S4C**).

180

### 181 **Pandemic CV-A24v strains have acquired a capsid residue that enhances sialic acid binding**

182 After its emergence in 1970 in Singapore, the pathogenic CV-A24 “variant” initially circulated only in  
183 Southeast Asia but started to spread globally in 1985, causing numerous AHC outbreaks and two  
184 pandemics. Concurrently, CV-A24 strains that do not belong to the “variant” clade and do not cause  
185 AHC continued to circulate worldwide and are sporadically found in stool samples. To understand  
186 whether the presence of Tyr<sup>250</sup> correlates with the ability of CV-A24v to cause AHC, we compared the  
187 Sia-binding sites between “variant” and “non-variant” strains. To classify these strains, we constructed  
188 a phylogenetic tree of all available complete CV-A24 VP1 sequences (**Fig. S4D**), originating from  
189 isolates collected worldwide during seven decades, including the first AHC outbreak in 1970 and the  
190 two subsequent pandemics that started in 1985 and 2002 (**Fig. 4D**). This tree showed that of the 226  
191 strains, 189 belong to the “variant” clade, which is delineated by the earliest AHC-causing strain  
192 EH24/70 that was isolated in Singapore in 1970 (**Fig. 4E**). A comparison of amino acid frequencies in  
193 the Sia-binding site revealed that most “non-variant” strains, as well as the first AHC strain EH24/70  
194 have a phenylalanine at VP1 position 250, whereas all “variant” strains isolated since the first AHC  
195 pandemic possess VP1 Tyr<sup>250</sup> (**Fig. 4E**). Such a genetic change could result from a population bottle-  
196 neck that “variant” strains may have undergone when invading a new target tissue. However, the  
197 absence of this residue in the “ancestral” strain EH24/70 suggests that Tyr<sup>250</sup> was not present during the  
198 initial tropism switch, but was adopted by its pandemic descendants in consequence of positive  
199 selection in the eye. The selective pressure to maintain this residue might be due to a more prominent  
200 role of Sia for infection in the ocular tissue to which AHC strains have adapted. To establish whether  
201 Tyr<sup>250</sup> promotes Sia usage, we constructed an infectious cDNA clone of CV-A24v strain 110390 and  
202 mutated Tyr<sup>250</sup> to Phe. This mutant and the wildtype virus were equally infectious in HeLa cells, in  
203 which Sia does not play a role. In HCE cells, however, wildtype CV-A24v was more infectious than  
204 the Tyr<sup>250</sup>Phe mutant (**Fig. 4F**) and this difference was abolished by NA treatment. Consistently, the  
205 wildtype virus bound better to Sia-expressing HCE cells than the Tyr<sup>250</sup>Phe mutant (**Fig. 4G**),  
206 indicating that Tyr<sup>250</sup> increases the capacity of CV-A24v to bind Sia. Together, these data demonstrate  
207 that the tropism switch of CV-A24 towards the eye was followed by the acquisition of a residue that  
208 enhances Sia-binding, an adaptation which coincides with the emergence of pandemic CV-A24v.

209

### 210 **Discussion**

211 This study provides new insights into the receptor requirements of CV-A24v and reveals that a subtle  
212 change in the engagement of a secondary attachment receptor, Sia, may have promoted the adaptation  
213 of a pathogen to a new niche. Although VP1 Tyr<sup>250</sup> is not a prerequisite for Sia binding (**Fig. 4F**), our  
214 results show that the presence of this residue can enhance Sia binding. Possibly together with other  
215 mutations outside the Sia-binding site, the adoption of an enhanced Sia-binding capacity by pandemic  
216 AHC-causing strains may have been a crucial evolutionary step in becoming a well-adapted ocular  
217 virus that can rapidly spread worldwide and cause AHC pandemics. Sia is also a receptor for several

218 other ocular viruses such as adenovirus type 37, enterovirus D70 and influenza A virus (21–23),  
219 suggesting that Sia is important particularly for infection of the eye. Improved Sia-binding properties  
220 may promote CV-A24v attachment to and infection of conjunctival cells, thereby increasing the viral  
221 load in the eye and enhancing transmission. Since CV-A24v is believed to be transmitted via hand-to-  
222 eye contact, the fate of CV-A24v after the initial disposition into the eye might be largely determined  
223 by its capacity to attach to the conjunctival tissue before it is cleared by the continuous draining of tear  
224 film through the nasolacrimal duct. A weak and dynamic interaction with highly sialylated mucus  
225 proteins might facilitate this initial attachment and rapidly secure virions in the mucus layer, without  
226 eliminating virus mobility.

227

228 While the emergence of pandemic CV-A24v may have been promoted by the acquisition of VP1  
229 Tyr<sup>250</sup>, it remains unknown what has caused the initial adaptation of CV-A24 to the eye. The genetic  
230 change underlying this tropism switch may be a combination of multiple synergistic mutations, which  
231 could reside in the capsid-coding region, non-structural genes, or non-coding regulatory elements in the  
232 viral genome. For CV-A24v, it has been reported that the emergence of the AHC-causing CV-A24v  
233 “variant” was accompanied by a loss of amino acid diversity (**Table S2**), probably as a result of a  
234 population bottleneck (24). Consequently, numerous genetic differences exist between “variant” and  
235 “non-variant” strains. Such changes in amino acid diversity also occurred at several CV-A24 capsid  
236 sites that interact with ICAM-1 (**Table S3**), some of which may have caused subtle changes in the  
237 engagement of ICAM-1 that facilitated ocular tropism. Thus, the identification of ICAM-1-binding  
238 residues in CV-A24v may help future studies investigating whether changes in ICAM-1 binding have  
239 contributed to the earliest manifestation of AHC.

240

241

242 **Materials and Methods**

243 Extended methods and information about cell lines, viruses (including construction of CV-A24v  
244 110390 infectious cDNA clones), chemicals and reagents, are described in **SI Materials and methods**.

245

246 **Electron microscopy.** Cryo-EM grids were prepared by applying 3  $\mu$ l of purified CV-A24v (10  
247 mg/ml) to 400 mesh lacey grids coated in a 3 nm carbon film (Agar Scientific, UK). The sample was  
248 left to adsorb for 30 seconds before most of the sample was blotted away manually. On-grid binding of  
249 the receptor was performed by applying 3  $\mu$ l of ICAM-1 D1-D2 (9.85 mg/ml) to the pre-blotted, virus-  
250 containing grid, and leaving for 30 seconds before blotting and freezing using a Leica EM GP plunge  
251 freeze (Leica Microsystems) device. The Leica EM chamber temperature was set to 8 °C with 80 %  
252 relative humidity and liquid ethane was used for sample vitrification. Grids were glow discharged for  
253 30 seconds prior to application of the samples. CV-A24v – ICAM-1 D1-D2 data was collected on an  
254 FEI Titan Krios (ABSL, University of Leeds) transmission electron microscope at 300 kV, using a total  
255 electron dose of 60 e-/Å<sup>2</sup> and a magnification of 75,000x. The final calibrated object sampling was  
256 1.065 Å/pixel. A total of 2643 exposures were recorded using the EPU automated acquisition software  
257 on a FEI Falcon III direct electron detector operating in linear mode. Each exposure movie had a total  
258 exposure of one second and contained 40 frames. Image processing, model building and refinement are  
259 described in **SI Materials and methods**.

260

261 **Infectivity assays.** Cells were incubated with virus for 1 hour at 37°C or, where indicated, on ice. After  
262 virus binding, cells were washed once with PBS (ice-cold PBS was used after virus binding on ice).  
263 Cells were supplied with fresh medium and incubated at 37°C for a total of 8 hours, which represents a  
264 single replication cycle. In virus production assays, cells were subjected to three freeze/thaw cycles and  
265 virus titers were determined by end-point dilution. Crystal violet staining was performed 4 days post-  
266 infection. In neutralization assays, cells were pretreated with antisera or soluble receptors for 45  
267 minutes at 37°C. Unless otherwise indicated, neuraminidase treatments were performed by incubating  
268 cells with a 1:30 dilution of A. urefaciens NA in serum-free medium for 1 hour at 37°C. Treatments  
269 with periodate, which oxidizes vicinal diols in glycans, was performed by incubation of cells with 5  
270 mM NaIO<sub>3</sub> in PBS for 1 hour on ice.

271

272 **Immunofluorescence assays.** Cells were fixed by submersion in a 4% paraformaldehyde solution for  
273 15 minutes. Fixed cells were stained with 1:2000 diluted mouse monoclonal anti-dsRNA (J2; English  
274 and Scientific Consulting). Cells were examined by confocal microscopy (Leica SPE-II) and the  
275 number of infected cells was quantified with ImageJ.

276

277 **Virus binding assays.** HCE cells were successively incubated with NA for 1 hour at 37°C, 1% BSA in  
278 PBS for 10 min on ice, virus for one hour on ice and washed three times with ice-cold PBS. RNA was  
279 isolated from cells using the NucleoSpin RNA Isolation Kit (Macherey-Nagel, Ref.No. 740955.250).  
280 cDNA was generated using the TaqMan Reverse Transcription Reagents kit (Applied Biosystems,  
281 Ref.No. N8080234). Quantitative PCR was performed using the Roche Lightcycler 480 SYBR Green I

282 Master kit (Roche, Ref.No. 04 887 352 001). For binding assays with HC0597 cells, CV-A24v was <sup>35</sup>S-  
283 labelled as described previously (11), followed by treatment with soluble proteins for 1 h at 37°C.  
284 Adherent HC0597 cells were detached (with phosphate-buffered saline [PBS]–0.05% EDTA, Merck)  
285 and recovered in growth medium at 37°C. After 1h, 100.000 cells/sample were washed and diluted in  
286 50µl binding buffer (HC0597 media + 0,5% Bovine serum albumin (Roche, Stockholm, Sweden) +  
287 HEPES pH 7.4 (EuroClone, Milan, Italy)) before the addition of 5000 <sup>35</sup>S-labeled CVA24v virions/cell.  
288 Cells were washed and the radioactivity of the cells was measured using a Wallac 1409 scintillation  
289 counter (Perkin-Elmer, Waltham, MA).

290

291 **Bio-layer interferometry.** Biolayer interferometry was performed with the Octet® Red 384 (ForteBio)  
292 using biotinylated ICAM-1 and LAMP-1. Streptavidin sensors were loaded with a 2 µg/ul solution of  
293 each protein for 15 min. Association of viruses to the sensor was performed for 60 min.

294

295 **Phylogenetic analysis.** All available CV-A24(v) sequences spanning the entire VP1 protein were  
296 downloaded from Genbank (January 1, 2017) and aligned using the ClustalW (1.6) algorithm  
297 implemented in MEGA version 7, followed by manual refinement. A phylogenetic tree of VP1  
298 sequences was constructed using the neighbor-joining method and the maximum composite likelihood  
299 method implemented in MEGA version 7. The phylogenetic tree was visualized using Figtree version  
300 1.4.3.

301

302 **Data availability.** The cryo-EM reconstruction and atomic model are deposited in the Electron  
303 Microscopy Data Bank (EMDB) and Protein Data Bank (PDB) under the accession codes EMD-3880  
304 and PDB-6EIT. VP1 sequences are available in Genbank under accession numbers MG272373,  
305 MG272374 and MG272375.

306

### 307 **Acknowledgements**

308 The authors thank Dieter Blaas for providing ICAM-1-specific antiserum (supersup). Funding was  
309 provided by the Netherlands Organization for Scientific Research grant NWO-VICI-91812628 (to  
310 F.J.M.v.K.), by the German Research Foundation grant SFB685 (to T.S. and G.Z.) and the Wellcome  
311 Trust PhD Studentship support 102572/B/13/Z (to D.L.H.). All Electron Microscopy was performed in  
312 the Astbury Biostructure Laboratory, which was funded by the University of Leeds and the Wellcome  
313 Trust (108466/Z/15/Z).

314

315 **References**

- 316 1. Ghazali O, et al. (2003) An outbreak of acute haemorrhagic conjunctivitis in Melaka, Malaysia.  
317 Singapore Med J 44(10):511–516.
- 318 2. Kurokawa M, Rai SK, Ono K, Gurung R, Ruit S (2006) Viral investigation of acute  
319 hemorrhagic conjunctivitis outbreak (2003) in Nepal using molecular methods. Southeast Asian  
320 J Trop Med Public Health 37(5):904–910.
- 321 3. Oh M, et al. (2003) Acute Hemorrhagic Conjunctivitis Caused by Coxsackievirus A24 Variant,  
322 South Korea, 2002. Emerg Infect Dis 9(8):8–10.
- 323 4. Measroch V, Gear J, Faerber GI (1951) Studies in Poliomyelitis: the isolation of a coxsackie-  
324 like virus from the faeces of apparently healthy Bantu infants. South African Med J 25(25).
- 325 5. Kono R, et al. (1972) Pandemic of new type of conjunctivitis. Lancet 1(7762):1191–1194.
- 326 6. Mirkovic RR, Schmidt NJ, Yin-Murphy M, Melnick JL (1974) Enterovirus Etiology of the  
327 1970 Singapore Epidemic of Acute Conjunctivitis. Intervirology 4:119–127.
- 328 7. Miyamura K, et al. (1988) The first epidemic of acute hemorrhagic conjunctivitis due to a  
329 coxsackievirus A24 variant in Okinawa, Japan, in 1985-1986. Japanese J Med Sci Biol 41:159–  
330 174.
- 331 8. Ishiko H, et al. (1992) Phylogenetic analysis of a coxsackievirus A24 variant: The most recent  
332 worldwide pandemic was caused by progenies of a virus prevalent around 1981. Virology  
333 187(2):748–759.
- 334 9. Lévêque N, Huguet P, Norder H, Chomel J-J (2010) Les Enterovirus responsables de  
335 conjonctivite aiguë hémorragique. Médecine Mal Infect 40(4):212–218.
- 336 10. Rossmann MG, He Y, Kuhn RJ (2002) Picornavirus-receptor interactions. Trends Microbiol  
337 10(7):324–331.
- 338 11. Nilsson EC, Jamshidi F, Johansson SMC, Oberste MS, Arnberg N (2008) Sialic acid is a  
339 cellular receptor for coxsackievirus A24 variant, an emerging virus with pandemic potential. J  
340 Virol 82(6):3061–8.
- 341 12. Zocher G, et al. (2014) A Sialic Acid Binding Site in a Human Picornavirus. PLoS Pathog  
342 10(10):e1004401.
- 343 13. Baggen J, et al. (2016) Enterovirus D68 receptor requirements unveiled by haploid genetics.  
344 Proc Natl Acad Sci 113(5):1399–1404.
- 345 14. van de Stolpe A, van der Saag PT (1996) Intercellular adhesion molecule-1. J Mol Med (Berl)  
346 74(1):13–33.
- 347 15. Shafren DR, Dorahy DJ, Greive SJ, Burns GF, Barry RD (1997) Mouse Cells Expressing  
348 Human Intercellular Adhesion Molecule-1 Are Susceptible to Infection by Coxsackievirus  
349 A21. 71(1):785–789.
- 350 16. Greve JM, et al. (1989) The major human rhinovirus receptor is ICAM-1. Cell 56(5):839–47.
- 351 17. Bergelson JM, et al. (1997) Isolation of a common receptor for Coxsackie B viruses and  
352 adenoviruses 2 and 5. Science 275(5304):1320–1323.
- 353 18. Xiao C, et al. (2005) The crystal structure of coxsackievirus A21 and its interaction with  
354 ICAM-1. Structure 13(7):1019–33.

- 355 19. Varghese JN, et al. (1997) Structural evidence for a second sialic acid binding site in avian  
356 influenza virus neuraminidases. *Proc Natl Acad Sci U S A* 94(22):11808–12.
- 357 20. Bakkens MJG, et al. (2016) Coronavirus receptor switch explained from the stereochemistry of  
358 protein–carbohydrate interactions and a single mutation. *Proc Natl Acad Sci*:E3111–E3119.
- 359 21. Arnberg N, Edlund K, Kidd AH, Wadell G (2000) Adenovirus type 37 uses sialic acid as a  
360 cellular receptor. *J Virol* 74(1):42–8.
- 361 22. Alexander D a., Dimock K (2002) Sialic Acid Functions in Enterovirus 70 Binding and  
362 Infection. *J Virol* 76(22):11265–11272.
- 363 23. Belser J a, Rota P a, Tumpey TM (2013) Ocular tropism of respiratory viruses. *Microbiol Mol*  
364 *Biol Rev* 77(1):144–56.
- 365 24. Smura T, et al. (2014) The Evolution of Vp1 Gene in Enterovirus C Species Sub-Group That  
366 Contains Types CVA-21, CVA-24, EV-C95, EV-C96 and EV-C99. *PLoS One* 9(4):1–16.
- 367

368 **Figure legends**

369

370 **Figure 1.** ICAM-1 is an essential CV-A24 receptor. (A) Yields of infectious virus after a single  
371 replication cycle. Sia-deficient HAP1 CMAS<sup>KO</sup> cells were treated with antibodies against enterovirus  
372 receptors (ICAM-1, DAF, integrin  $\alpha 2$ , PVR, CAR, integrin  $\alpha \nu \beta 3$ , and PSGL-1) or soluble receptor  
373 (VLDL-R) and infected at 37 °C with CV-A24v 110387. (B) Schematic representation of ICAM-1  
374 showing immunoglobulin-like domains 1-5 (D1-D5) and the two sites targeted by CRISPR/Cas9  
375 (gRNA 1 and 2). Knockout was accomplished by disrupting a 1489 bp region of ICAM1 encoding the  
376 transmembrane domain (TM), either by excision of this region or by introducing a frameshift mutation.  
377 (C) HeLa-R19 ICAM-1<sup>KO</sup> transfected with plasmid encoding ICAM-1 cDNA were exposed to virus and  
378 yields of infectious virus were measured after a single replication cycle. (D) Bio-layer interferometry  
379 analysis of virus binding to either ICAM-1 or negative control receptor LAMP-1. (E) Relative levels of  
380 CV-A24v 110390 bound to primary conjunctival cells with expanded lifespan (HC0597), in the  
381 presence of ICAM-1 D1D5 or negative control receptor CAR D1. (F) HeLa-R19 cells were infected  
382 and yields of infectious virus were determined after a single replication cycle. Dashed lines (A, C and  
383 F) represent virus input levels (T=0). Error bars (A, C, E and F) represent the mean  $\pm$  SEM of 3-4  
384 biological replicates. (G) HeLa-R19 cells were infected with seven CV-A24v clinical isolates, two CV-  
385 A24 “non-variant” strains and ICAM-1-dependent (CV-A21, RV-14) or CAR-dependent (CV-B3)  
386 control viruses, followed by crystal violet staining of surviving cells.

387

388 **Figure 2.** The structure of CV-A24v in complex with ICAM-1. (A) Enlarged tilted view of density  
389 denoted by a black triangle in (B), containing the corresponding atomic model. ICAM-1 D1 binds in  
390 the ‘canyon’ located at the quasi three-fold axis. (B) The cryo-EM reconstruction of CV-A24v in  
391 complex with ICAM-1 (D1D2) viewed down the icosahedral two-fold axis. VP1-3 (3.6 $\sigma$ ), D1 (1 $\sigma$ ) and  
392 D2 (0.6 $\sigma$ ). (C) Typical example of the cryo-EM electron density of VP1-3 and D1 domain. (D)  
393 Radially colored isosurface representation of CV-A24v in complex with D1 (grey) viewed down the  
394 icosahedral two-fold axis (left). The stereographic projection of the viral surface (right), where the  
395 polar angles  $\theta$  and  $\phi$  represent latitude and longitude, respectively. Amino acids which interact with  
396 ICAM-1 D1 are located at the floor and wall of the canyon (blue) and are circled in white. The radial  
397 colouring key is shown in angstroms. (E) Surface representation of the EM-derived atomic model for  
398 the quasi three-fold axis of CV-A24v (grey) and ICAM-1 D1 (pink), with residues forming salt bridges  
399 labelled and coloured in respect to their interacting partners. The left panel shows the surface of CV-  
400 A24v and the right panel shows the surface of ICAM-1 D1 that interacts with CV-A24v. Residues  
401 forming salt bridges are coloured according to charge (red is negative, blue is positive) and capsid  
402 residues that hydrogen bond with ICAM-1 are dark grey. (F) Overview of electrostatic interactions  
403 shown in (E) between ICAM-1 (pink) and CV-A24v (blue) with potential hydrogen bonds denoted as  
404 dotted black lines and EM density as a green mesh.

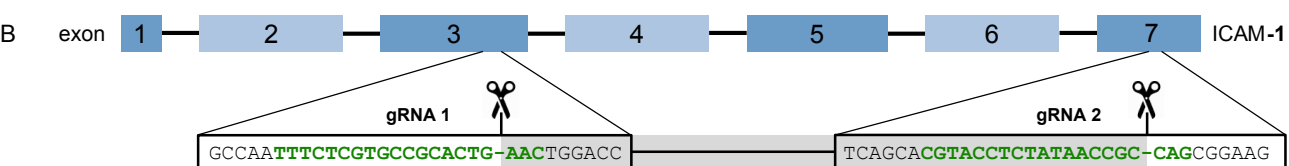
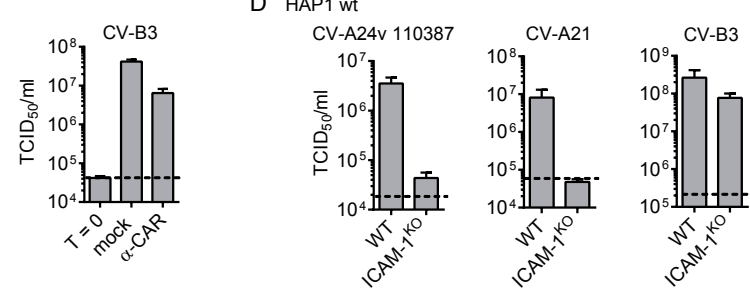
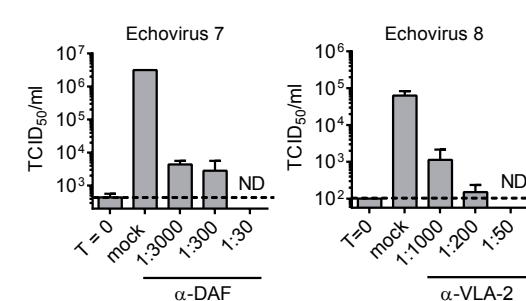
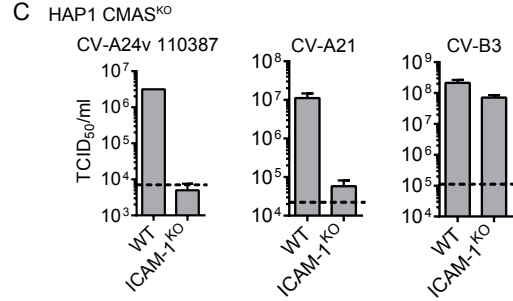
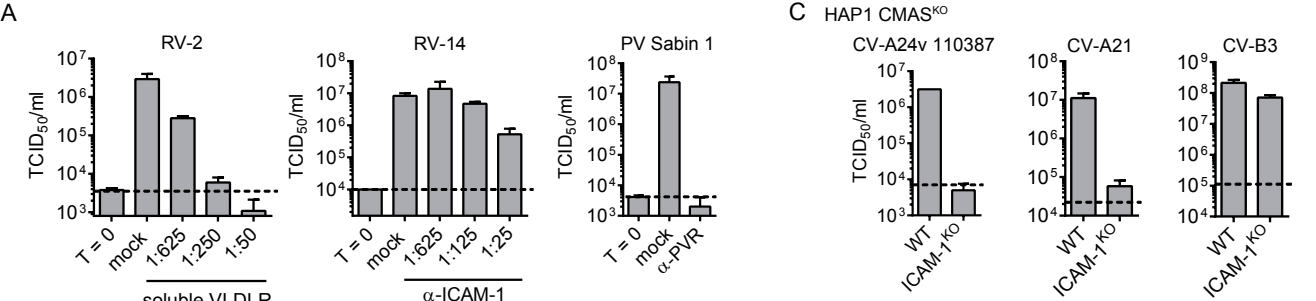
405

406 **Figure 3.** Sia is an attachment receptor supporting ICAM-1-mediated CV-A24v infection. (A) HCE  
407 cells were treated with a mixture of *A. urefaciens* and *V. cholerae* NA (1:30), infected with CV-A24v

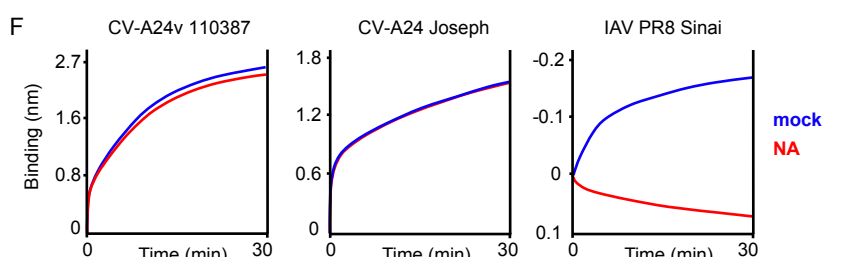
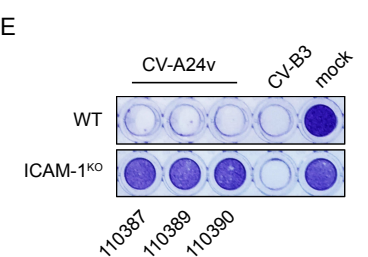
408 110387 on ice (0°C) or at 37°C, followed by qPCR analysis of viral RNA levels after a single  
409 replication cycle. (B) NA-treated cells were infected with CV-A24v 110387 and yields of infectious  
410 virus were determined after a single replication cycle. (C) NA-treated HCE cells were infected on ice  
411 with CV-A24v, Sia-dependent enterovirus D68 (EV-D68) and Sia-independent CV-B3, followed by  
412 staining of dsRNA (green) and nuclei (blue). Shown are representative confocal micrographs.  
413 Percentage values denote mean  $\pm$  SEM of three technical replicates, normalized to mock. (D and E)  
414 HCE cells were treated with a mixture of *A. urefaciens* and *V. cholerae* NA (1:30) and infected on ice.  
415 After incubation with virus, viral RNA levels were determined by qPCR either directly (E) or after a  
416 single replication cycle (D). (F) Levels of radioactively labeled CV-A24v 110390 bound to NA-treated  
417 (*V. cholerae* 10 mU/ml) primary conjunctival cells with expanded lifespan (HC0597) on ice (0°C) or at  
418 37°C. Dashed lines (A, B and D) represent virus input levels (T=0). Error bars represent the mean  $\pm$   
419 SEM of 3 (A, B, D and E) or 8 (F) biological replicates. P-values (A and F) were calculated by an  
420 unpaired two-sided T-test; \*P<0.05; \*\*P < 0.01; \*\*\*P < 0.001.

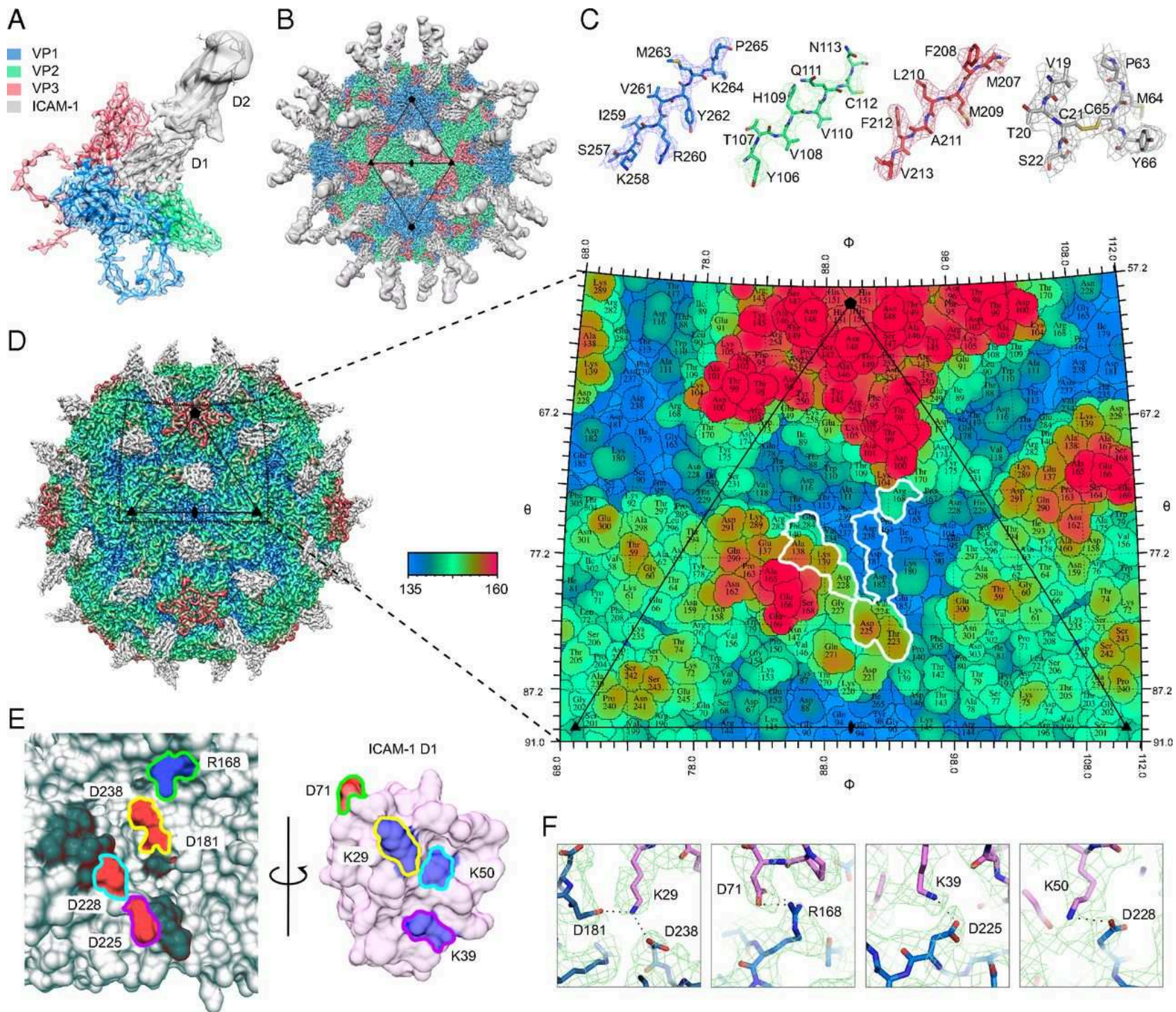
421

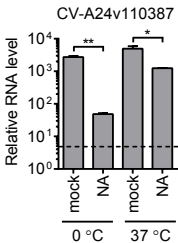
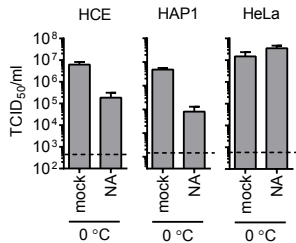
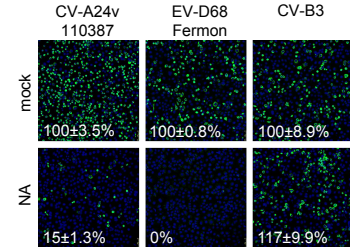
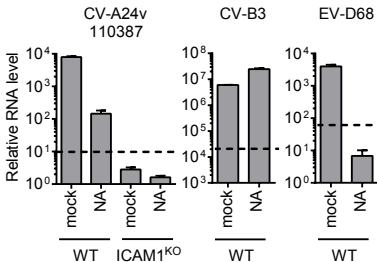
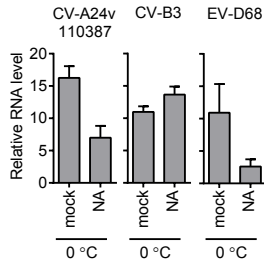
422 **Figure 4.** Pandemic CV-A24v strains have acquired a capsid residue that enhances sialic acid binding.  
423 (A) NA-treated HCE cells were infected on ice, followed by staining of infected cells with a dsRNA  
424 antibody (green) and nuclei with DAPI (blue). Percentage values denote mean  $\pm$  SEM of three  
425 technical replicates, normalized to mock. (B) Amino acid sequence alignment of tested CV-A24  
426 strains, with the residue unique for non-variant strains highlighted in red. (C) Binding site for Sia  
427 (orange) in CV-A24v 110390 (PDB 4Q4X), showing that the 5-N-acyl group of Sia is stabilized by two  
428 hydrogen bonds (dashed lines). Two adjacent VP1 proteins are colored grey and blue, respectively. Red  
429 spheres represent water molecules. Oxygen and nitrogen atoms are colored red and blue, respectively.  
430 (D) Geographic origins of non-AHC- (red) and AHC-causing (purple, light blue, blue) CV-A24 strains  
431 of which complete VP1 sequences are available, with circle sizes proportional to the number of  
432 isolates. (E) Phylogenetic tree of CV-A24 isolates, showing on the right side the frequencies of amino  
433 acids in the Sia-binding site among the indicated number of strains. Frequency plots were generated  
434 with WebLogo. Residues at VP1 position 250 are highlighted in gray. (F) HCE cells were treated with  
435 NA and infected on ice with CV-A24v 110390 or the VP1 Y250F mutant, followed by staining of  
436 dsRNA (green) and nuclei (blue). Quantifications shown at the bottom denote mean  $\pm$  SEM of four  
437 technical and two biological replicates. Images shown in A and F are representative confocal  
438 micrographs. (G) HCE cells were treated with a mixture of *A. urefaciens* and *V. cholerae* NA (1:30)  
439 and incubated with virus on ice, followed by qPCR analysis of bound virus. Error bars represent the  
440 mean  $\pm$  SEM of 3 biological replicates. P-values (F and G) were calculated by an unpaired two-sided  
441 T-test; ns P  $\geq$  0.05; \*\*P < 0.01; \*\*\*\*P < 0.0001.



cell line	allele	17853	19373
HeLa clone 11	1	GCCAA <b>TTTCTCGTGCCGCACTG</b> <del>A</del> AACTGGACC.....TCAGCACGTACCTCTATAACCGC-CAGCGGAAG	
	2	GCCAA <b>TTTCTCGTGCCGCACTG</b> -----GACC.....TCAGCACGTACCTCTATAACCGC-CAGCGGAAG	
	3	GCCAA <b>TTTCTCGTGCCGCACTG</b> ----- 1489 nt -----CAGCGGAAG	
HAP1 clone 2	1	GCCAA <b>TTTCTCGTGCCGCACTG</b> XXX----- 1486 nt -----CAGCGGAAG	
	2	GCCAA <b>TTTCTCGTGCCGCACTG</b> ----- 1489 nt -----CAGCGGAAG	
HAP1 CMAS <sup>ko</sup> clone 8	1	GCCAA <b>TTTCTCGTGCCGCACTG</b> ----- 1489 nt -----CAGCGGAAG	
	2	GCCAA <b>TTTCTCGTGCCGCACTG</b> -AACTGGACC.....TCAGCACGTACCTCTATAACCGC <b>C</b> CAGCGGAAG	
HCE clone 2	1	GCCAA <b>TTTCTCGTGCCGCACTG</b> ----- 1489 nt -----CAGCGGAAG	
	2	GCCAA <b>TTTCTCGTGCCGCACTG</b> ----- 1489 nt -----CAGCGGAAG	





**A** HCE cells**B** CV-A24v 110387**C** HCE cells**D** Virus replication in HCE**E** Virus binding to HCE**F** Virus binding to HC0597 cells